(Received 13 November 2025, Accepted 4 December 2025, Scheduled 26 December 2025)

Design and Analysis of Interior Permanent-Magnet Machine for Improving Reluctance Torque and Heat Dissipation

Yujie Tang, Jingfeng Mao, and Junqiang Zheng*

School of Electrical Engineering and Automation, Nantong University, Nantong 226019, China

ABSTRACT: This paper proposes an Interior Permanent Magnet (IPM) machine for electric vehicles, which features excellent heat dissipation performance and maximizes the utilization of reluctance torque. The inverted triangular structure design, combined with multi-layer flux barriers and ventilation auxiliary slots, effectively increases the saliency ratio and enhances the reluctance torque. The rotor self-ventilation slots significantly expand the heat dissipation area, improve the heat dissipation performance under steady-state operation, and extend the service life of the rotor. In addition, the performance evaluation of the IPM machine is conducted, covering back-EMF, torque performance, dq-axis inductances, rotor stress and deformation, as well as thermal performance. This work provides guidance and reference for machine design.

1. INTRODUCTION

Electric vehicles require higher torque performance, wider speed range, high efficiency, and excellent heat dissipation performance. IPM machines are widely used in this field due to their unique structural characteristics [1–5]. Fully utilizing the high reluctance torque performance of the IPM topology structure can effectively improve electromagnetic torque. Thereby enabling better performance of the drive motor [6–8]. However, machines operating at high speeds often experience higher temperature rises, which will reduce their lifespan. By designing different flux barriers and auxiliary slots, the electromagnetic and mechanical performance of the machine can be effectively improved [9–11]. Therefore, utilizing the magnetic reluctance torque brought by the IPM topology structure to enhance electromagnetic torque has important research significance.

The electromagnetic torque of IPM consists of two components. Namely, permanent-magnet (PM) torque is generated by the interaction of the air-gap magnetic field and stator armature reaction magnetic field [12–14], while reluctance torque is generated by the asymmetry of the magnetic circuit of the d-axis and q-axis [14–16]. Different rotor topologies have a significant impact on torque performance and heat dissipation performance.

Nowadays, numerous scholars have conducted extensive research on this type of motor, proposed many new rotor designs, and carried out analyses [17]. An axial modular combined permanent magnet-assisted synchronous reluctance motor is proposed. Compared to traditional interior permanent magnet synchronous machines and permanent magnet-assisted synchronous reluctance machines, this machine offers advantages such as low torque ripple, reduced eddy current loss, and a high power factor [18]. A new rotor topology for permanent magnet-assisted synchronous reluctance machines is introduced. The d-axis of this design shifts from the traditional d-axis, which effectively reduces torque ripple and enhances output power [19]. It combines symmetric flux barriers with asymmetric magnetic poles, and utilizing the Magnetic Field Shifting (MFS) effect, it achieves the maximum values of both PM torque and reluctance torque at similar current angles. This enhances the machine's output torque [20]. By adopting a hybrid approach using ferrite and neodymium-iron-boron, the two permanent magnets are asymmetrically arranged on both sides of the "U"-shaped magnetic barrier. This arrangement enhances the reluctance torque, improves the utilization rate of the permanent magnets, and reduces their cost.

This paper introduces a new rotor topology that combines inverted triangular slots with a K-type magnetic barrier structure. This design effectively boosts the saliency ratio of the permanent magnet machine, enhances the reluctance torque component, and thereby increases the electromagnetic torque. By utilizing the ventilation and heat dissipation features of the inverted triangular slots, the machine's temperature rise during operation is managed, leading to excellent heat dissipation performance.

2. THEORETICAL ANALYSIS

Ignoring the saturation of the motor core avoids inductance parameter variations caused by magnetic circuit nonlinearity, thereby enabling rapid acquisition of the basic characteristics of reluctance torque. Neglecting hysteresis losses and eddy current losses helps focus on the core driving mechanism of reluctance torque, preventing interference from loss calculations in magnetic field solutions. The mathematical model of the permanent magnet-assisted synchronous reluctance machine in the dq reference frame is developed. The machine space vector diagram is shown in Fig. 1.

* Corresponding author: Junqiang Zheng (zjq@ntu.edu.cn).

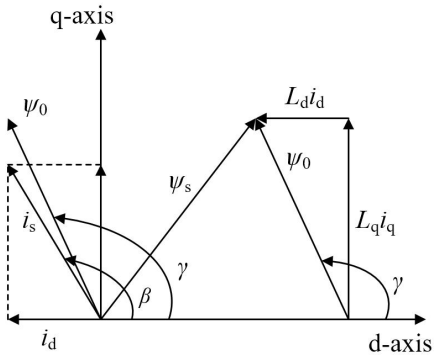

FIGURE 1. Space vector diagram of permanent magnet assisted synchronous reluctance machine.

In the vector diagram, i_s represents the stator DC space vector, while i_d and i_q denote the d-axis component and q-axis component, respectively. L_d and L_q represent the direct-axis inductance and quadrature-axis inductance, respectively. ψ_{PM} represents the flux linkage generated by the rotor permanent magnets; ψ_0 is the flux linkage induced by i_s; ψ_s is the resultant flux linkage of ψ_{PM} and ψ_0; β is the angle between i_s and d-axis; γ is the angle between ψ_0 and d-axis.

From Fig. 1, it is evident that due to the difference in inductance between the d-axis and q-axis of the machine, and the q-axis inductance is greater than the d-axis inductance, the magnetic flux produced by the stator winding current does not align with the phase of the stator current space vector. ψ_0 lags behind i_s in phase, and as the ratio of the machine's q-axis inductance to d-axis inductance (salient pole ratio) increases, the phase difference between ψ_0 and i_s becomes larger. Therefore, in synchronous reluctance machines, increasing the salient-pole ratio can reduce the phase difference between the voltage and current, and enhance the machine's reluctance torque.

The voltage equations, flux linkage equations, and electromagnetic torque equation of the permanent magnet-assisted synchronous reluctance machine are as follows:

$$u_d = \frac{d\psi_d}{dt} - \omega\psi_q + Ri_d \tag{1}$$

$$u_q = \frac{d\psi_q}{dt} - \omega\psi_d + Ri_q \tag{2}$$

$$\psi_d = L_d i_d + \psi_{PM} \tag{3}$$

$$\psi_q = L_q i_q \tag{4}$$

$$T_{em} = p\left(\psi_{PM} i_q + \left(L_d - L_q\right) i_d i_q\right) \tag{5}$$

where u_d and u_q are the direct-axis and quadrature-axis components of the voltage space vector; ψ_d and ψ_q are the direct-axis and quadrature-axis components of the stator flux linkage; ω is rotational angular velocity; R is the winding phase resistance; T_{em} is the electromagnetic torque; p is the number of poles.

According to the operating principle of the machine, the simplified formula for the electromagnetic torque of the permanent magnet-assisted synchronous reluctance machine is as follows:

$$T_{em} = p\psi_{PM} i_s \sin\beta + \frac{1}{2} p\left(L_d - L_q\right) i_s^2 \sin 2\beta \tag{6}$$

From the torque formula of permanent magnet machines, it can be seen that to improve the torque output capability of permanent magnet-assisted synchronous reluctance machines, efforts can be made in two aspects. First, increase the PM flux linkage to enhance the PM torque. Second, increase the difference between the d-axis inductance and q-axis inductance to improve the reluctance torque, thereby boosting the electromagnetic torque.

3. TOPOLOGY AND OPTIMIZATION

Figure 2 clearly illustrates the rotor topology of the novel permanent magnet synchronous machine proposed in this paper. Its main design feature is embedding permanent magnets into V-shaped grooves, optimizing both magnetic and mechanical properties. This paper introduces a structure that combines an inverted triangular opening with multiple layers of K-type magnetic flux barriers. By precisely controlling the distribution of the rotor magnetic flux path, the rotor salient pole ratio is significantly improved, directly increasing the magnetic reluctance torque contribution. This results in more stable torque output under various operating conditions.

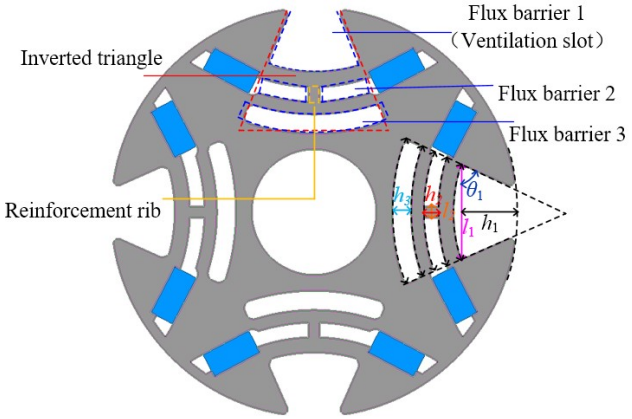

FIGURE 2. Structural characteristics of the proposed rotor.

The reinforced rib structure inside the magnetic flux barrier is a key design feature. It not only compensates for the decrease in rotor stiffness caused by traditional magnetic flux barriers and enhances the rotor's mechanical strength against centrifugal force and vibration, but also reduces magnetic flux leakage by optimizing the magnetic field distribution in the barrier, achieving simultaneous improvements in electromagnetic and mechanical performance. The triangular groove on the rotor's outer surface offers two benefits: It reduces the rotor's weight through reasonable material removal to lower the moment of inertia, and it increases the heat dissipation area to speed up heat transfer and improve thermal stability. Additionally, the study iteratively adjusts parameters such as the angle between the permanent magnet and the V-groove, embedding depth, and circumferential position using multi-objective optimization algorithms to better explore the potential of magnetic reluctance torque. Some basic parameters are listed in Table 1.

During the optimization process, the objective of this study is to maximize both torque and reluctance torque. Due to the large number of rotor parameters, we use a comprehensive sensitivity

TABLE 1. Main parameters of the IPM machine.

Design parameters	Values
Rated current (A)	10
Number of poles	4
Number of stator slots	18
Rated speed (rpm)	5000
Outer diameter of stator (mm)	95
Inner diameter of stator (mm)	54
Axial length of stator core (mm)	60
Inner diameter of rotor (mm)	16
Air gap (mm)	0.9

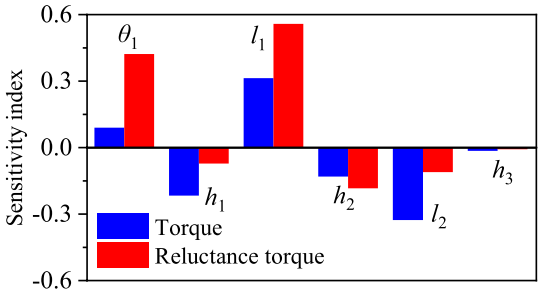

FIGURE 3. Sensitivity analysis of two optimization objectives.

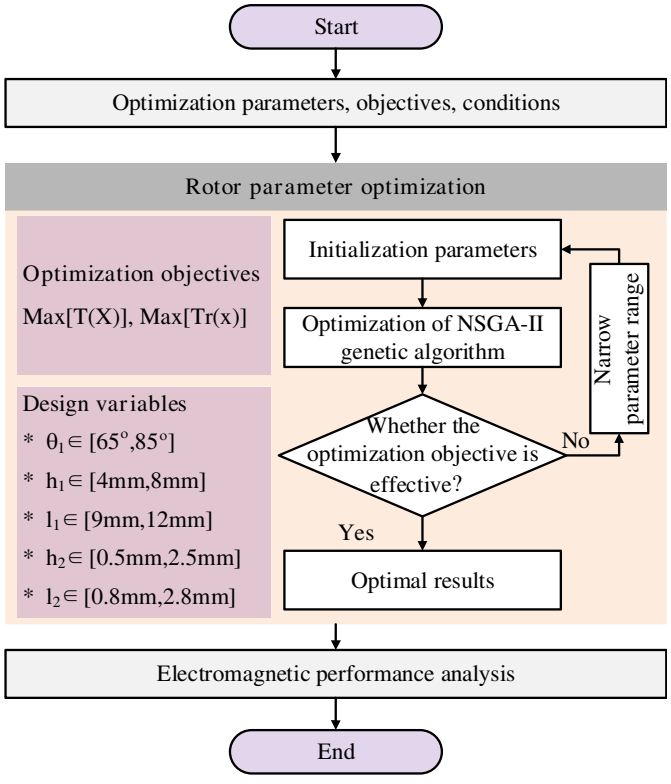

FIGURE 4. Multi-objective flow sheet.

analysis method to select key parameters. Table 2 displays the sensitivity indicators for each parameter, and Fig. 3 presents a histogram of torque and reluctance torque to clearly show how design variables impact them.

TABLE 2. Sensitivity analysis results.

Optimization Variables	Sensitizer	
	Torque	Reluctance torque
θ_1	0.087	0.421
h_1	−0.221	−0.075
l_1	0.311	0.557
h_2	−0.135	−0.188
l_2	−0.332	−0.114
h_3	−0.017	−0.011

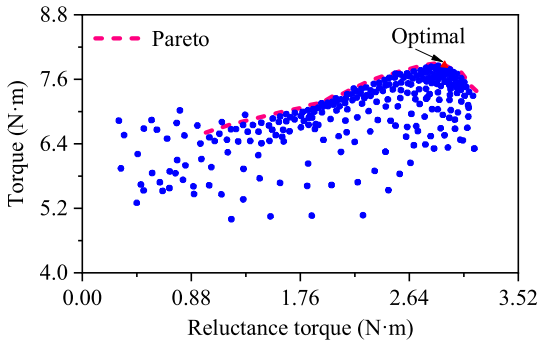

FIGURE 5. Multi-objective optimization result for the IPM machine.

The rotor parameters greatly influence the machine's torque, requiring multi-objective optimization methods to find the best design settings. As shown in Fig. 4, the NSGA-II genetic algorithm is used for system parameter selection, and Pareto front analysis helps balance competing objectives. The optimization focuses on five main geometric parameters (rotor triangular groove elevation angle θ_1, triangle groove depth h_1, triangle groove bottom width l_1, width of the flux barrier h_2, width of magnetic barrier reinforcement rib l_2), aiming to maximize torque and reluctance torque.

Figure 5 shows the results of the multi-objective optimization for the IPM machine, with red scatter points indicating the Pareto front. The machine marked by the red triangle is ultimately selected. At this point, the optimal torque is 7.66 N · m, and the reluctance torque is 2.89 N · m.

4. PERFORMANCE ANALYSIS

Figure 6 shows the no-load back-EMF waveform and harmonic spectrum of the IPM machine. The waveform is approximately saddle-shaped, which helps to improve the utilization of voltage and enhance the dynamic response of the machine. From its harmonic spectrum, it can be seen that there is a significant 3rd order harmonic in the no-load back-EMF. It should be noted that the 3rd order harmonic does not affect the torque ripple.

The reluctance torque of a permanent magnet reluctance machine originates from the significant difference between the d-axis and q-axis inductances. As shown in Fig. 7, the d-axis inductance is notably higher than the q-axis inductance. This inductance difference causes a magnetic field distortion when current flows, generating a reluctance torque that helps improve the machine's torque output and performance.

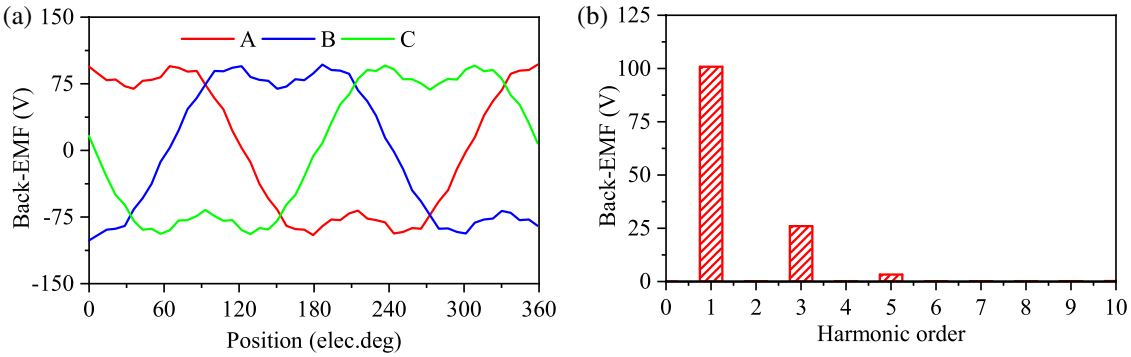

FIGURE 6. No-load back-EMF of the proposed machine. (a) Waveform. (b) Harmonic spectrum of A-phase winding.

Parameters	Traditional Rotor	Proposed Rotor
Electromagnetic torque (N · m)	7.4	7.7
Reluctance torque (N · m)	2.0	2.9
Torque ripple	5.1%	4.4%
Rotor volume (mm^3)	97382	69576
Heat dissipation area (mm^2)	29872.7	42860.1
Core loss (W)	39.1	32.6
Solid loss (mW)	53.3	125.3

TABLE 3. Comparison of performance indicators.

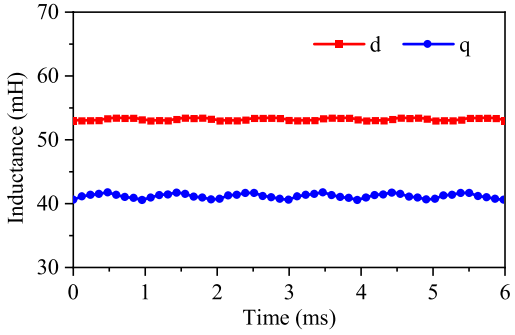

FIGURE 7. dq-axis inductance curve of the proposed machine.

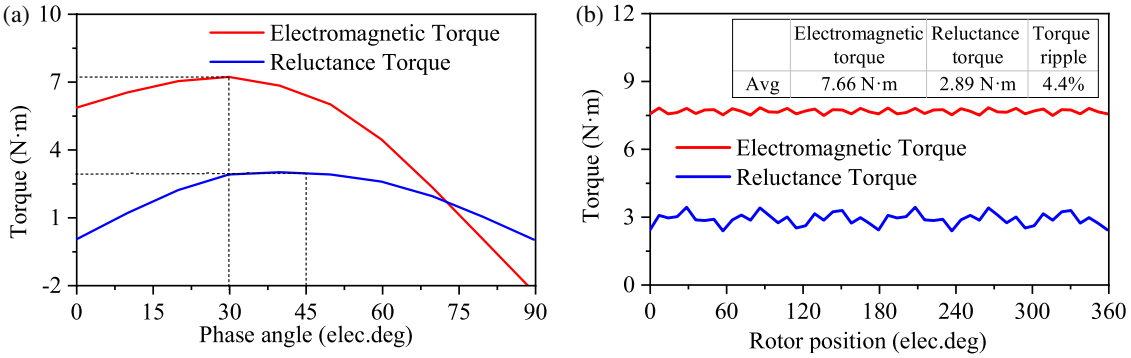

FIGURE 8. Torque curve of the proposed machine. (a) Torque varies with phase angle. (b) Torque varies with rotor position.

The variation of the electromagnetic torque and reluctance torque of the PM machine with the current phase angle and rotor position is shown in Fig. 8(a). It can be observed that when the current phase angle is 0° (elec. deg), i.e., when the control strategy of $Id = 0$ is adopted, no net average reluctance torque is produced, but there is still a small torque ripple, as shown in Fig. 9. At a phase angle of 45° (elec. deg), the reluctance torque reaches its maximum and then drops, the reluctance torque can be given by

$$T_r = \frac{U^2}{2\omega}\left(\frac{1}{X_q} - \frac{1}{X_d}\right)\sin 2\beta \tag{7}$$

where T_r is the reluctance torque, U the terminal voltage, ω the rotational angular velocity, X_q the q-axis reactance, X_d the q-axis reactance, and β the rotor position.

The total electromagnetic torque reaches its maximum at a phase angle of 30° (elec. deg), where the reluctance torque accounts for about 38%. In addition, Fig. 8(b) shows the torque performance curve at the ideal operating point, where the electromagnetic torque and the reluctance torque are 7.66 N · m and 2.89 N · m, respectively, with a low torque ripple.

Figure 10 shows the magnetic flux density map of a permanent magnet machine, where the teeth have a relatively saturated magnetic flux density of 1.6 T, and the maximum magnetic flux density of the yoke is 1.8 T. The magnetic flux density of the rotor magnetic barrier is 1.8 T, matching the stator magnetic circuit, and at this point, the magnetic barrier is also saturated, allowing for a large reluctance torque.

The stress and deformation analysis of the IPM machine is illustrated in Fig. 11. Evidently, the main stress distribution areas are the reinforcing rib part between the connection

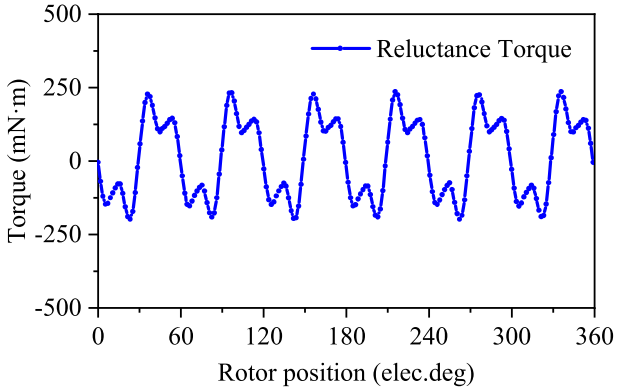

FIGURE 9. Reluctance torque at current phase angle of 0°.

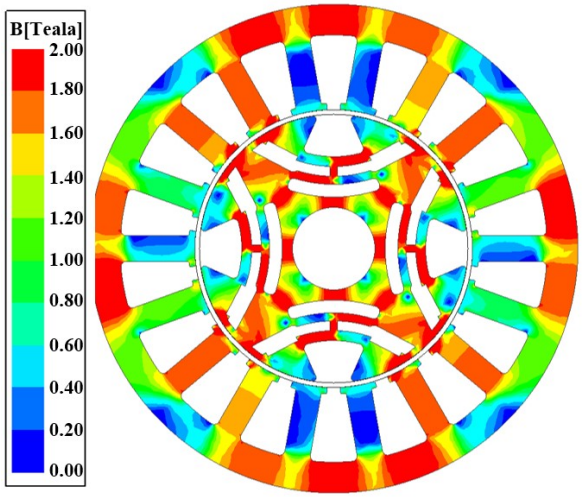

FIGURE 10. Magnetic flux density of the proposed machine.

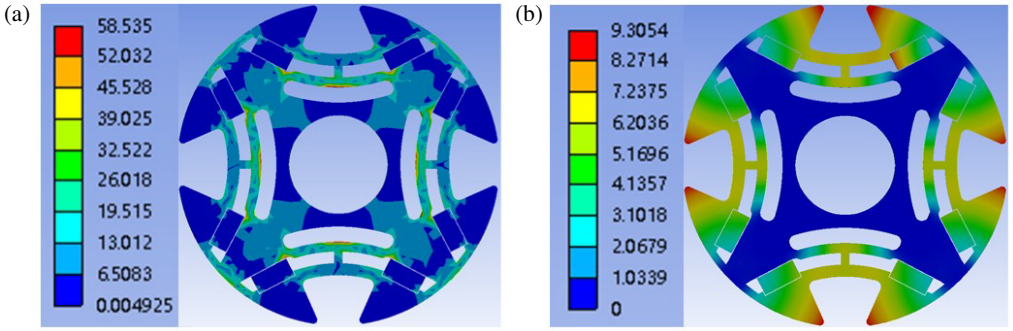

FIGURE 11. Stress and deformation of the proposed machine. (a) Stress. (b) Deformation.

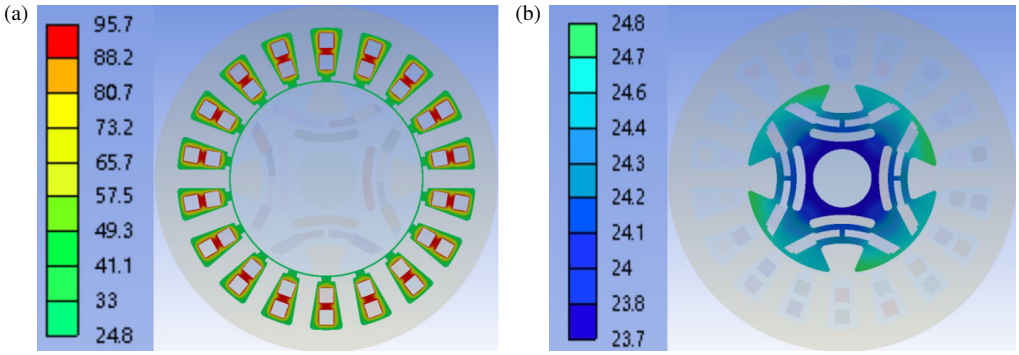

FIGURE 12. Thermal of the proposed machine. (a) Stator. (b) Rotor.

bridge between PMs and the flux barrier. Its maximum stress is 58.5 MPa, which meets the stress limit of conventional structural steel (150 MPa). The main deformation area is also the reinforcing rib part between the flux barriers. Its maximum deformation is 9.3 µm. The deformation range is much smaller than the width of the air gap. The use of inverted triangles and multi-layer magnetic flux barriers effectively increases the stress level of the rotor and enhances its mechanical strength.

Figure 12 exhibits the 2D thermal analysis of the IPM machine. Due to the inverted triangular ventilation slots and multiple layers of auxiliary slots, the heat dissipation area is effectively increased, which improves the service life of the rotor. The heat generated by the rotor part of the proposed IPM machine is much smaller than that of the stator, the proposed topology structure presents good heat dissipation performance.

This paper compares the proposed new rotor topology with the traditional slotless rotor structure. The results are shown in Table 3. It can be seen that the proposed inverted triangular structure, combined with multi-layer flux barriers, effectively increases the reluctance torque component, thereby improving the electromagnetic torque. Compared with the traditional rotor, the proposed topology reduces the volume by 28.55%,

which lowers the motor weight, and increases the heat dissipation area by 43.47%, effectively enhancing the self-heat dissipation performance of the rotor.

5. CONCLUSIONS

This paper proposes a novel type of IPM machine for new energy-electric vehicles. It provides a large reluctance torque and has good heat dissipation performance. The design of multi-layer magnetic barriers improves the salient pole ratio of the rotor, thereby enhancing the reluctance torque. In addition, the ventilation properties of the open slot are organically combined, and a rotor self-ventilation slot is designed to improve the heat dissipation performance.

The electromagnetic performance of the machine shows that the proposed multi-layer flux barrier structure significantly improves the reluctance torque of the machine, thereby increasing the total electromagnetic torque. In addition, the thermal analysis structure indicates that the presence of self-ventilation slots significantly enhances the heat dissipation performance of the machine and improves its service life. Stress analysis reveals that the structural strength of the rotor has been improved, which can meet the design requirements.

ACKNOWLEDGEMENT

This work was supported in part by the National Natural Science Foundation of China (52307061), the Natural Science Research Program of Jiangsu Colleges and Universities under Grant (23KJB470033), and the Postgraduate Research & Practice Innovation Program of Jiangsu Province (SJCX24_2005).

REFERENCES

[1] Chen, H., A. M. El-Refaie, and Y. Liu, "Investigation of a PM flux-modulated motor with mechanical flux-weakening solution for wide speed-range operation in traction applications," *IEEE Transactions on Industrial Electronics*, Vol. 71, No. 8, 8646–8657, Aug. 2024.

[2] Xu, M., W. Zhao, J. Ji, Q. Chen, and G. Liu, "Auxiliary notching rotor design to minimize torque ripple for interior permanent magnet machines," *IEEE Transactions on Industrial Electronics*, Vol. 71, No. 10, 12 051–12 062, Oct. 2024.

[3] Li, S., C. Di, and X. Bao, "Axis-shifted machines with hybrid rotors considering forward and reverse operations," *IEEE Transactions on Magnetics*, Vol. 59, No. 11, 1–6, Nov. 2023.

[4] Li, S., W. Tong, S. Wu, and R. Tang, "General analytical model for electromagnetic-thermal bi-directional coupling of IPM motors in electric vehicles considering different rotor structures," *IEEE Transactions on Vehicular Technology*, Vol. 73, No. 11, 16 470–16 480, Nov. 2024.

[5] Du, G., H. Yan, N. Li, L. Li, Y. Chen, G. Lei, and J. Zhu, "Four rotor structures for high speed interior permanent magnet motor considering mechanical, electromagnetic and thermal performance," *IEEE Transactions on Transportation Electrification*, Vol. 11, No. 1, 2595–2608, Feb. 2025.

[6] Dai, L., J. Gao, S. Niu, and S. Huang, "Multi-electromagnetic performance optimization of double-layer interior permanent magnet synchronous machine," *IEEE Transactions on Industrial Electronics*, Vol. 71, No. 11, 14 535–14 545, Nov. 2024.

[7] Jansson, E., T. Thiringer, and E. A. Grunditz, "Influence of flux barrier shape and mechanical constraints on field-weakening performance in double-layer interior permanent magnet machines," *IEEE Transactions on Energy Conversion*, Vol. 40, No. 1, 30–42, Mar. 2025.

[8] Ji, Y., Y. Li, and Q. Lu, "Novel asymmetric rotor hybrid interior permanent magnet synchronous machines for torque density and PM utilization ratio improvement," *IEEE Transactions on Industry Applications*, Vol. 61, No. 6, 9159–9171, Nov.–Dec. 2025.

[9] Wang, B., D. Wang, C. Peng, C. Wang, C. Xu, and X. Wang, "Interior permanent magnet synchronous machines with composed T-shaped notching rotor," *IEEE Transactions on Industrial Electronics*, Vol. 71, No. 6, 5519–5529, Jun. 2024.

[10] Ajamloo, A. M., A. Ghaheri, M. N. Ibrahim, and P. Sergeant, "Investigation of different pole configurations in new asymmetric permanent magnet synchronous reluctance machines," *IEEE Transactions on Magnetics*, Vol. 61, No. 9, 1–6, Sep. 2025.

[11] Wang, L., X. Zhang, J. Wu, M. Wang, W. Hu, H. Geng, and X. Pang, "Multi-objective optimization design of a segmented asymmetric V-type interior permanent magnet synchronous motor," *IEEE Transactions on Magnetics*, Vol. 61, No. 1, 1–12, Jan. 2025.

[12] Lee, J.-H., K.-Y. Yoon, and B.-I. Kwon, "Optimization of a double-layer flared-shaped IPMSM for torque ripple reduction," *IEEE Access*, Vol. 13, 165 999–166 011, 2025.

[13] Cheng, Y., L. Ding, T. Zhao, and S. Cui, "Design and optimization of electric vehicle traction motor considering rotor topology and manufacturing uncertainty," *IEEE Transactions on Industrial Electronics*, Vol. 71, No. 5, 5034–5044, May 2024.

[14] Bi, Y., J. Huang, H. Wu, W. Fu, S. Niu, and X. Zhao, "A general pattern of assisted flux barriers for design optimization of an asymmetric V-shape interior permanent magnet machine," *IEEE Transactions on Magnetics*, Vol. 58, No. 9, 1–4, Sep. 2022.

[15] Nobahari, A., A. Vahedi, and R. Nasiri-Zarandi, "A modified permanent magnet-assisted synchronous reluctance motor design for torque characteristics improvement," *IEEE Transactions on Energy Conversion*, Vol. 37, No. 2, 989–998, Jun. 2022.

[16] Mohammadi Ajamloo, A., A. Ghaheri, M. N. Ibrahim, and P. Sergeant, "Principle of torque-axis alignment in new asymmetric PM synchronous reluctance machines: Towards less-rare-earth pm machines," *IEEE Transactions on Transportation Electrification*, Vol. 11, No. 2, 6392–6405, Apr. 2025.

[17] Liu, Z., Y. Hu, J. Wu, B. Zhang, and G. Feng, "A novel modular permanent magnet-assisted synchronous reluctance motor," *IEEE Access*, Vol. 9, 19 947–19 959, 2021.

[18] Mohammadi, A. and S. M. Mirimani, "Design and analysis of a novel permanent magnet assisted synchronous reluctance machine using finite-element-method," in *2020 11th Power Electronics, Drive Systems, and Technologies Conference (PEDSTC)*, 1–5, Tehran, Iran, 2020.

[19] Gao, Y., D. Jiang, H. Zhu, B. Mao, and Y. Liu, "Design optimization of asymmetric permanent magnet assisted bearingless synchronous reluctance motor," *IEEE Transactions on Energy Conversion*, Vol. 40, No. 2, 1644–1654, Jun. 2025.

[20] Xie, Y., J. Shao, S. He, B. Ye, F. Yang, and L. Wang, "Novel PM-assisted synchronous reluctance machines using asymmetrical rotor configuration," *IEEE Access*, Vol. 10, 79 564–79 573, 2022.